Composites Science and Technology 123 (2016) 276–285

Contents lists available at ScienceDirect

Composites Science and Technology

journal homepage: http://www.elsevier.com/locate/compscitech

A facile assembly of 3D robust double network graphene/polyacrylamide architectures via γ-ray irradiation

Ting Zhu, Kunyue Teng, Jie Shi, Lei Chen, Zhiwei Xu*

Key Laboratory of Advanced Braided Composites, Ministry of Education, School of Textiles, Tianjin Polytechnic University, Tianjin 300387, PR China

ARTICLE INFO

Article history:
Received 23 June 2015
Received in revised form
1 October 2015
Accepted 5 November 2015
Available online 10 November 2015

Keywords:
Graphene/polyacrylamide architectures
Polymers
Nano composites
Heat treatment
Mechanical properties

ABSTRACT

Addressed herein was a facile one-step method to obtain three-dimensional (3D) robust double network graphene/polyacrylamide architecture (DNGA) which was constructed by polyacrylamide-modified graphene network and polyacrylamide (PAM) network via γ-ray irradiation. The application of γ-ray irradiation technique promoted the efficient preparation of 3D graphene networks for its characteristic of high energy. The resultant DNGA with an ordered double network macroporous structure achieved high compressive strength of 1.45 MPa, which was quadruple compared with that in previous reports. After being thermal-annealed at 800 °C in N_2 atmosphere, the obtained DNGA/N_2 with stable porous structure exhibited an excellent Young's modulus of 2.93 MPa, which was triple higher than that reported in the latest literature. Considering the outstanding compressive property of DNGA and DNGA/N_2, a series of analyses supported the strengthening mechanism of the double network. The present results suggest that the convenient synthetic approach can act as a potential candidate for fabricating high-strength 3D graphene materials, which may provide insight into a meaningful development of large-scale and low-cost preparation of 3D graphene networks.

1. Introduction

Graphene, the truly two-dimensional (2D) planar with one-atom-thick of sp^2 carbon atoms, has attracted tremendous attention in all manner of disciplines (i.e., physics, chemistry, biology, device fabrication, etc.) due to its impressive surface area and prominent electronic, optical, thermal and mechanical properties [1–3]. However, due to the strong van der Waals interactions and high inter-sheet junction contact resistance between isolated graphene sheets, the irreversible agglomeration or restacking of graphene sheets severely suppress the intrinsical performance of individual graphene sheets, simultaneously diminish the accessible surface area of graphene sheets [4,5]. For its better utilization, graphite oxide (GO), a graphene derivative which can be mass-produced and easily surface functionalized, is widely used as a raw material to manufacture graphene materials in bulk or in composite [6–8].

Up to now, great interest has been focused on constructing 3D graphene networks to improve the dispersion and orientation, which are vastly evolved with many new techniques and becoming desirable in advanced applications, such as catalysis, electronics, sensors, energy conversion, storage device, displays and reinforced composites [9–13]. 3D graphene networks, such as graphene foams, graphene sponges, graphene architectures and graphene aerogels, can be obtained principally by template-directed method and self-assembly technology, which include chemical vapor deposition on matrix foams [14,15], using ice templates by lyophilization [16–18], calcinations and etching various templates [19,20], or indeed lyophilizing a variety of hydrogels [21–25]. Among them, the chemical vapor deposition is a valid method to prepare high purity products, but it usually involves bottleneck problems like high temperature, inefficiency and valuableness. Other methods can be carried out at a relatively low temperature, especially the approaches of freeze-drying ice templates and assembling graphene oxide, which have been demonstrated to be the most popular methods for preparing 3D graphene networks. However, these networks suffer from inferior mechanical property, complicated processes, small-scale production and poisonous reagents, which cause precautions and high cost in industrial production [26]. Relatively weak mechanical property of the networks, which results from the interactions with the individual graphene oxide sheets such as electrostatic interaction, hydrogen bonding,

* Corresponding author.
E-mail address: xuzhiwei@tjpu.edu.cn (Z. Xu).

http://dx.doi.org/10.1016/j.compscitech.2015.11.007
0266-3538/

π−π interaction or inclusion interaction, is a main challenge to overcome. In this context, it is worth mentioning that Zhu and his co-workers fabricated a series of 3D porous graphene sponges via using foam templates of soap bubbles by adjusting freezing rate, and their compressive stresses were from dozens to nearly five thousand of pascal [17]. Furthermore, Shi et al. reported a modified hydrothermal method to obtain macroporous graphene monoliths, and the maximum compressive stress and highest compressive modulus in his paper were 31.94 kPa and 42.29 kPa, respectively [24]. Presently, Yu et al. fabricated 3D graphene aerogels on the basis of in situ reduction-assembly method with improved compressive stress and compressive modulus of 146 kPa and 856 kPa, respectively, which possessed better mechanical property than those reported previously [27]. Nevertheless, the stable crosslinking which fundamentally endows 3D graphene networks with excellent mechanical strength is still urgent for the practical application. Therefore, a facile, efficient and economical method for the large-scale production of 3D graphene networks with high mechanical property is extremely desirable.

γ-Ray, as a mature non-contact technique to combine the simple processes, high purity and economic benefits for the preparation and modification of polymer and graphene, exhibits many other advantages, such as mild conditions, great penetrating power with ultra-uniformity and easy scaled-up production [28,29]. It is well-known that γ-ray irradiation technique is also a mild and convenient method to induce acrylamide (AM) monomers in situ polymerization to obtain polyacrylamide (PAM) hydrogel without any crosslinking agents [30,31]. In our previous works, γ-rays induced the intercalation, grafting and self-exfoliation of GO [28]. Zhang et al. described a simple route to prepare well-dispersed graphene in N,N-dimethylformamide by γ-rays at room temperature [32]. Recently, we developed a method to efficaciously graft PAM chains on the surface and between the layers of graphene oxide sheets, which inhibited the agglomeration of graphene oxide, and induced the reduction of modified graphene sheets simultaneously [33]. Combining with previous studies, the feasibility of constructing 3D graphene networks has been neglected. In virtue of great penetrating power and ultra-uniformity of γ-rays, 3D graphene networks could be constituted with the introduction of a special double network structure [34]. Owing to the interpenetrating polymer networks, the double network hydrogels possessed higher mechanical strength as compared to other gels [35]. To the best of our knowledge, γ-ray irradiation technique is still an unprecedented area for the preparation of 3D graphene networks, and there has been no similar report about the introduction of the double network to the 3D graphene networks. It is doable and imperative to investigate the properties and applications of double network graphene/polyacrylamide architectures (DNGA) prepared by γ-ray irradiation.

Herein, this study reported a straightforward route for in situ preparation of 3D robust DNGA via γ-ray irradiation. The microstructure formation mechanism of DNGA, effects of thermal treatment on the microstructure stability, degree of reduction, electrical conductivity and compressive property of the products were investigated systematically. Furthermore, the comparison of different 3D graphene networks on compressive property and preparation technics had been taken. Afterwards, the strengthening mechanism of double network in DNGA was discussed.

2. Experimental

2.1. Materials

Natural graphite flakes were provided by Qingdao Ruisheng Graphite Co., Ltd., China. The reagents (98% H_2SO_4, 85% H_3PO_4, 37.5% HCl, and 30% H_2O_2) and the analytical grade reagents ($KMnO_4$, AM) were the products of Tianjin Kermel Chemical Co., Ltd., China. The irradiation field (^{60}Co γ-ray source) was provided by Tianjin Institute of Technical Physics, China.

2.2. Preparation of DNGA and DNGA/N_2

Graphite oxide (GO) used in our experiment was prepared by the improved Hummers method, as reported elsewhere [36,37]. The concentration of GO aqueous dispersion was determined by freeze-drying small amount of suspension for 24 h and then weighing the dried GO. The standby GO aqueous dispersion was diluted to 10 mg/mL. In a typical experiment, 3.0 g AM powder was dissolved in 150 mL standby GO aqueous solution and the suspension was evenly stirred to obtain a uniform dispersion. Having been saturated with N_2 for 20 min to remove oxygen, the mixture was exposed to γ-ray using a ^{60}Co source under atmospheric pressure and ambient temperature in an airtight-capped glass vessel. The irradiation dose was accumulated to 100 kGy with a dose rate of 0.5 kGy/h. After irradiation, the resulting colloidal DNGA was washed by deionized water, and freeze-dried for 24 h. In addition, irradiated GO and PAM were also prepared as a control using the same process by irradiating GO solution with a concentration of 10 mg/mL or AM solution with a concentration of 20 mg/mL. To investigate the effects of thermal treatment, DNGA/N_2 was obtained by thermal-annealing process of DNGA at 800 °C for 2 h in nitrogen atmosphere with a heating rate of 5 °C/min.

2.3. Characterization

Fourier transform infrared (FTIR) spectra of the samples were recorded on a Bruker VECTOR-22 IR spectrometer using KBr pellets. The phases of samples were identified by X-ray diffraction (XRD) patterns with Cu Kα radiation (35 kV, 20 mA, λ = 1.54059 Å) in the continuous scanning mode. The 2θ scanning range was from 5° to 60 in steps of 0.017° with a collection time of 20 s per step. Atomic force microscopy (AFM) images were collected on a CSPM5500 scanning probe microscope in the tapping mode. Thermogravimetric analysis (TGA) was conducted with a Netzsch TG 209F1 under N_2 atmosphere with a heating rate of 10 °C/min. The degree of grafting (DG) was estimated by TGA for the pristine GO, PAM and DNGA, and was calculated using equation (1):

$$DG(\%) = \frac{R_G - R}{R_G - R_P} \times 100\% \quad (1)$$

Wherein, R_G, R and R_P represent the residual weight percentage (wt %) of pristine GO, DNGA and PAM pyrolysis, respectively. The Raman spectra were recorded on RENISHAW in Via Raman Microscope with an excitation wavelength of 514 nm and a power of 5 mW. X-ray photoelectron spectra (XPS) were recorded on PHI-5700 ESCA with Al Kα excitation radiation (1486.6 eV). The field emission scanning electron microscopy (SEM) was performed with a Hitachi S-4800 to represent the microscopic structure of the resulted samples. Densities of the DNGA samples were calculated by the weight of solid content excluding the weight of entrapped air divided by the volume of architectures. Unidirectional compression property of the samples were measured using an Instron 3369 testing machine (USA) at a constant strain rate of 1 mm/min. The electrical conductivity of the as-prepared DNGA and DNGA/N_2 was measured with a RTS-9 four-probe resistivity meter (Probes Tech., China) at room temperature by inserting four acicular probes into cuboidal samples with the dimension of 5 mm × 5 mm × 20 mm.

3. Results and discussion

The preparation approach of DNGA was shown in Fig. 1. N_2 was bubbled for 20 min to remove any dissolved oxygen, which lessened the oxidation of the ingredients and restrained termination of polymerization [30,38]. The homogeneous mixture solution was processed by γ-ray irradiation, resulting in the formation of different kinds of ions, excited molecules, electrons and active radicals. Previous studies showed that water was decomposed to hydrated electron (e^-_{aq}), hydroxyl radical (·OH) and hydrogen radical (·H) under γ-rays, as shown by the following formula (1) [39].

$$H_2O \xrightarrow{\gamma\text{-rays}} e^-_{aq} + \cdot H + H_2O_2 + H_3O^+ \quad (1)$$

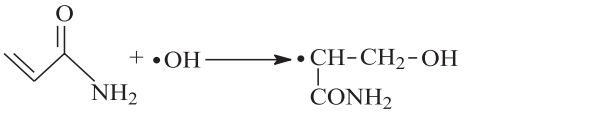

(2)

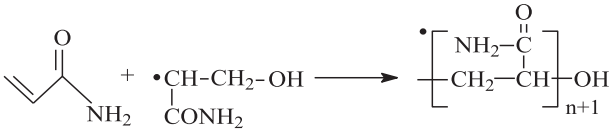

(3)

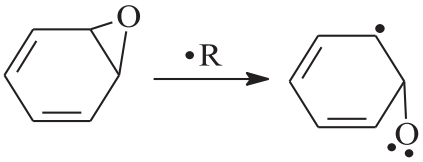

(4)

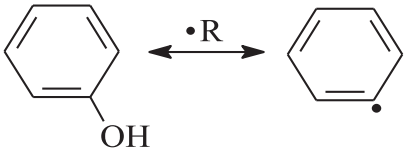

(5)

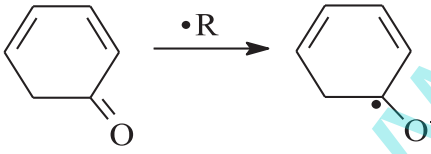

(6)

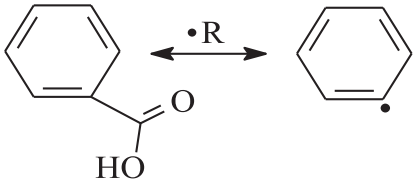

(7)

Among the species in (1), e^-_{aq}, ·OH and ·H are the most active particles which readily attack on other target molecules. The possible mechanism for the production of potential reactive radicals under the assistance of γ-rays was proposed in (2)–(7), where ·R represented reactive radicals like ·H and e^-_{aq} [40,41]. In (2), ·OH in the system induced the active sites of acrylamide for crosslinking. Then copolymerization of acrylamide was shown in (3). The e^-_{aq} and ·H were possibly capable of cleaving the C–O bond via four routes to form a carbon radical on the surface of graphene oxide, as shown in (4)–(7). These routes included the removal of epoxy, hydroxyl, carbonyl and carboxyl groups. The generation of reactive sites on both acrylamide monomers and graphene oxide sheets was leading to the propagation of the reaction. The activated radicals were responsible for modification, crosslinking and in situ polymerization simultaneously between graphene oxide nanosheets and acrylamide monomers [42]. The formation of DNGA was under the synergistic effects of three types of interactions: crosslinking within 3D graphene network and PAM network, and hydrogen-bond interaction between those two networks. The 3D graphene network was assembled by active site connections at the branch chains of the modified graphene and weak binding with the epoxy and carbonyl groups on the graphene oxide planes. Moreover, the 3D graphene network was intertwined with covalently crosslinked PAM network, thus resulting in a unique and stable double network architectures. Additionally, during γ-ray irradiation the generating reducing species (like ·H and e^-_{aq}) promoted the reduction process, and radical in situ polymerization assembly of robust DNGA was achieved. The morphology of the graphene nanosheets of GO and DNGA was analyzed using AFM (Fig. 2). Due to the extensive oxidation in the preparation procedure of GO, the thickness of graphene oxide nanosheet was ca. 1.5 nm. In contrast, the thickness for the nanosheet of DNGA was ca. 3.9 nm, which was thicker than GO sheets due to the attachment of PAM chains onto the surface of GO. The cross section images showed that the surface of DNGA sheets was smoother than that of a GO sheet.

FTIR spectroscopy is an informative measurement with qualitatively analyzing the compositional and structural information of the compounds, and determines polymerization and recombination of the products. The FTIR spectra of above samples were presented in Fig. 3(a). From the spectrum of pristine GO, it was obvious

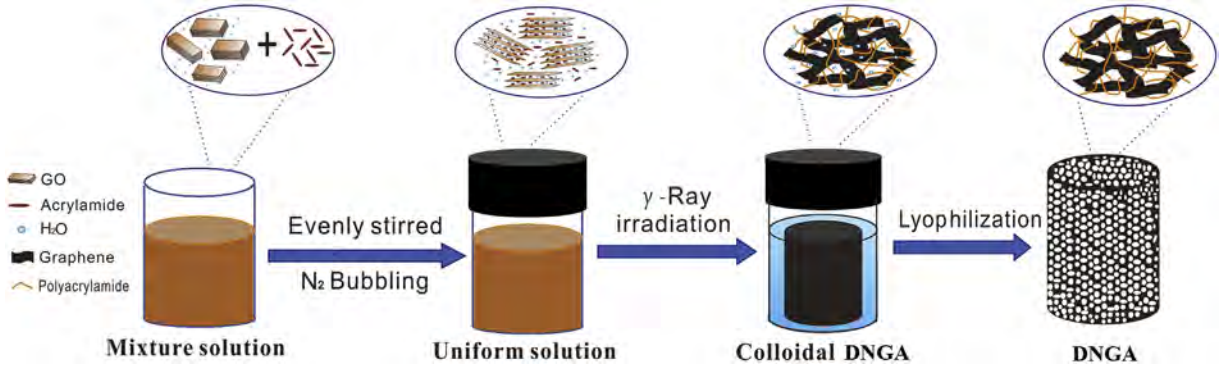

Fig. 1. Preparation process and formation mechanism of DNGA by γ-ray irradiation.

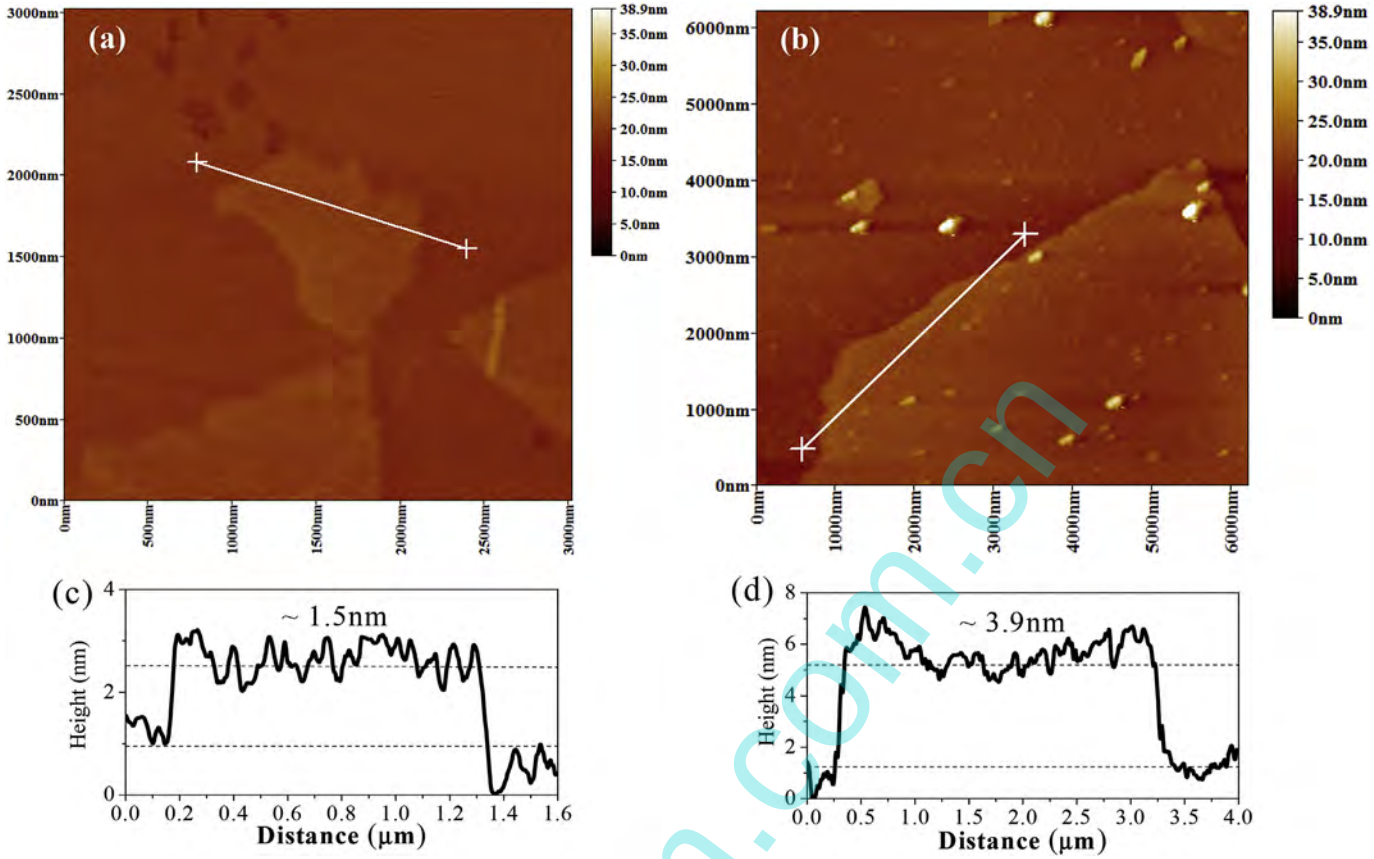

Fig. 2. Tapping mode AFM topographic images of graphene nanosheets from GO (a) and DNGA (b) sonicated for 30 min in deionized water, cross-section of graphene nanosheets from the sonicated GO (c) and DNGA (d).

that the characteristic peaks at 3380, 1723, 1398, 1174, and 1040 cm^{-1} represented for –OH stretching vibration, C=O stretching vibration, –OH deformation vibration, epoxy C–O and alkoxy C–O, respectively [29]. The peak at 1622 cm^{-1} was attributed to O–H bending vibration of absorbed water molecules and vibration of aromatic C=C. Due to the absence of scavengers of hydroxyl radicals, double-side effects will brought to GO: (i) reductive particles (e^-_{aq} and ·H) will attack on GO sheets, especially for the epoxy C–O and alkoxy C–O, to reduce GO in a certain extent; and (ii) ·OH in the system will introduce thermally labile oxygen groups like hydroxyl to GO sheets [42]. So the characteristic peak of –OH stretching vibration around 3400 cm^{-1} became remarkably distinct. A new peak appeared at 2926 cm^{-1} for the stretching modes of H bonded to an olefinic carbon for the formation of hydrogenated graphene after irradiation [43]. To further explain the influence of γ-rays on GO, the detailed C1s analysis of XPS spectra has been taken afterwards. In the spectrum of PAM, a series of characteristic peaks at 3190, 2940, 1679, 1572, 1457 and 1402 cm^{-1} were ascribed to N–H variable stretching, $-CH_2-$ stretching, C=O (amide I) stretching vibration, N–H deformation vibration for primary amide, $-CH_2-$ in-plane bending vibration and C–N stretching, respectively [31,44]. As for the DNGA, the

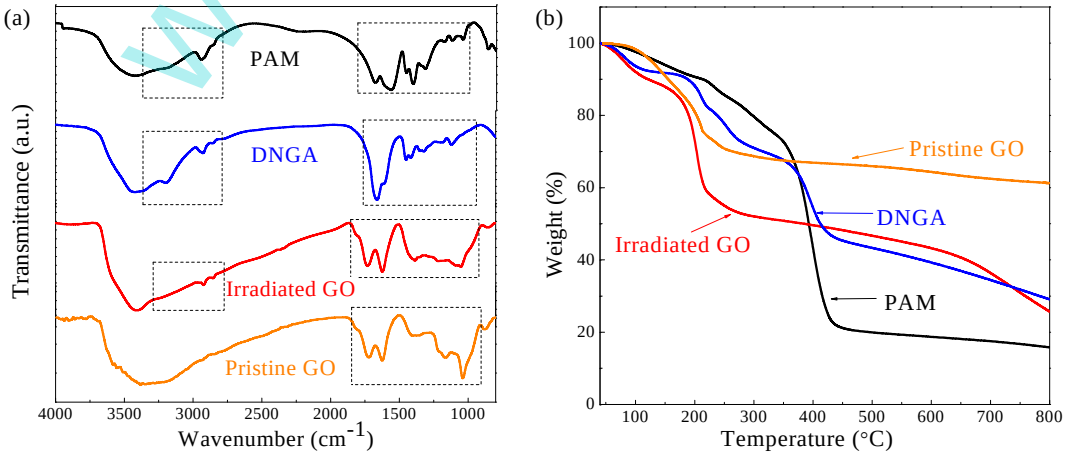

Fig. 3. FTIR spectra (a) and TGA thermograms (b) of PAM, DNGA, pristine GO and irradiated GO.

above bands belonging to GO and PAM were greatly decreased or even disappeared. The peaks at 3190, 1572, and 1121 cm^{-1} corresponding to the characteristic N–H stretching and NH_2 in-plane rocking of PAM were shifted to 3200, 1611, and 1115 cm^{-1}, respectively, in DNGA. Furthermore, the typical C=O stretching of the $-CO-NH_2$ group was shifted from 1679 cm^{-1} in PAM to 1661 cm^{-1} in DNGA. The obvious shifts of the absorption bands in DNGA fully indicated the successful polymerization and recombination, which manifested that 3D graphene network and PAM network were intertwined together and formed double network architectures.

Fig. 3(b) depicted the thermograms of PAM, DNGA, irradiated GO and pristine GO, respectively. The mass losses before 100 °C were assigned to the removal of water in the samples. For pristine GO, the TGA curve sharply decreased at around 200 °C, which presumably ascribed to the pyrolysis of labile oxygen-containing functional groups. From 250 to 650 °C, the stable oxygen functionalities were removed slowly and smoothly [45]. After irradiation, the thermal stability of irradiated GO under low temperature was found to be lowered in a certain degree because of the increased content of thermal unstable oxygen functional groups [42]. Owing to the amount of –OH increased significantly in irradiated GO, irradiated GO has a bigger weight loss compared with that of pristine GO from 150 to 250 °C [46]. As the organic carbon chains were decomposed around 440 °C, the residual weight of PAM was 21.52%. There are two clearly separated weight loss stages in the range of 180–300 °C and 350–450 °C for DNGA, corresponding to the breakage of polymer chains and the formation of amorphous carbon. The weight percentage of PAM in DNGA was about 69.53 wt%, as calculated according to equation (1), which demonstrated the quantitative compositions of DNGA. The overall residual weights at 800 °C were about 61.00, 25.41, 15.45 and 29.33 wt% for pristine GO, irradiated GO, PAM and DNGA, respectively. Because of the existence of graphene oxide, the weight loss percentage of DNGA was less than that of PAM at 600 °C. Even at 700 °C, the weight loss of DNGA was slightly close to that of

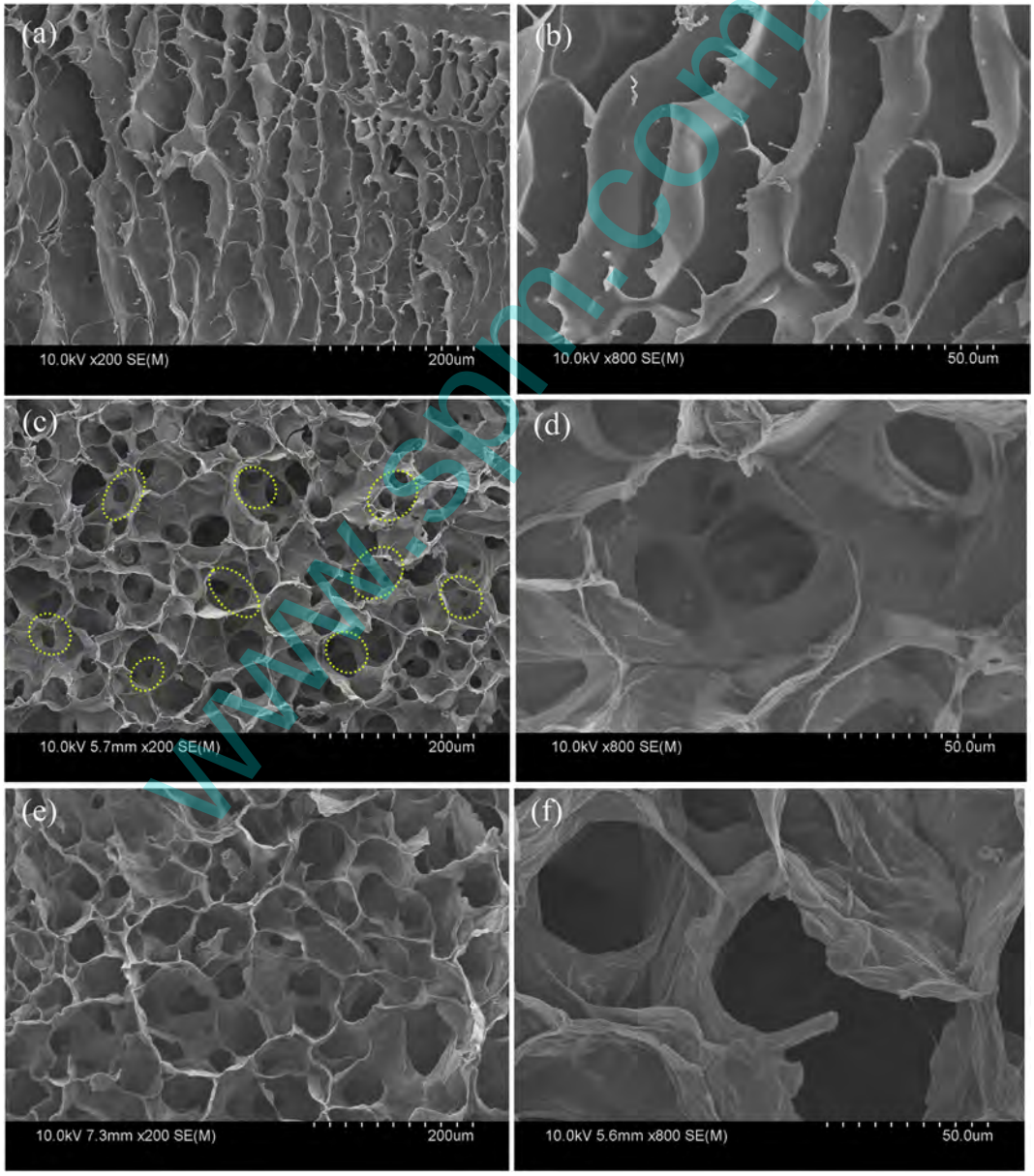

Fig. 4. SEM images of PAM (a–b), DNGA (c–d) and DNGA/N_2 (e–f) at different magnifications.

irradiated GO, which could be due to the fact that high chemical crosslinking fixated the slices of the modified graphene within DNGA. The analysis certified that the PAM chains partly improved the thermostability of DNGA before 400 °C, compared with pristine GO and irradiated GO. Meanwhile, after 400 °C the formation of polyacrylamide-modified graphene endowed DNGA more excellent heat-resistance than PAM.

As shown by SEM images of PAM in Fig. 3(a–b), the PAM displayed uniformly lamellar structure. Interestingly, the DNGA and DNGA/N_2 owned porous structure shown in Fig. 4(c–d). Whereas DNGA exhibited more compact porous structure, due to the presence of PAM network, which increased the relative cross-linking density of the porous structure [47]. After thermal-annealing process, the porous structures still existed in DNGA/N_2, except for the disappearance of some microporous structure which represented PAM porous structure. By SEM observation, the formation of highly stable porous structure in DNGA suggested that the double network was induced by crosslinked modified graphene and PAM via γ-ray irradiation. And even if decomposition and carbonization of polymer chains during thermal-annealing process, collapse did not occur because of the existence of graphene network. Firm skeleton strength of DNGA/N_2 betokened high Young's modulus, which was in line with the latter analysis of the double network of DNGA.

XRD, Raman spectroscopy and XPS were employed to understand the irradiation process of the mixture solution and effects of thermal treatment on DNGA. XRD patterns of all samples shown in Fig. 5(a) revealed the influence of functional groups on the interlayer spacing [29]. Due to the introduction of oxygen-containing functional groups, a characteristic peak of pristine GO around 10.36°corresponded to the interlayer spacing of 0.853 nm. Owing to the decrease of oxygen groups after irradiation, the interlayer distance of irradiated GO was obviously contractive, as shown in Fig. 5(a) [48]. The XRD pattern of PAM presented a broad noncrystalline diffraction peak from 14° to 27° [49]. However, for DNGA, the XRD pattern only showed a weak broad diffraction peak around 15–25°, and the diffraction peak of GO was disappeared. This phenomenon clearly demonstrated that modification of graphene by γ-ray irradiation made GO be peeled effectively, which led to the disappearance of the regular structure of graphene sheets. A broad noncrystalline diffraction peak centered at 20.8° of DNGA/N_2 presented the generation of amorphous carbon. The interlayer spacing reduction of DNGA/N_2 (0.424 nm) manifested that thermal treatment not only led to the disappearance of oxygenated functional groups, but also promoted the amorphous carbon attach between graphene network.

To investigate defects in graphene, Raman spectra of all samples were shown in Fig. 5(b). In the detection range, G peak (~1591 cm^{-1}) originating from in-plane vibration of sp^2 carbon atoms is a doubly degenerate phonon mode. There is also a defect or disorder induced D peak (~1357 cm^{-1}), which is caused by introducing sp^3 carbon originating from a double resonance Raman process involving iTO phonon as well as electrons [50]. The

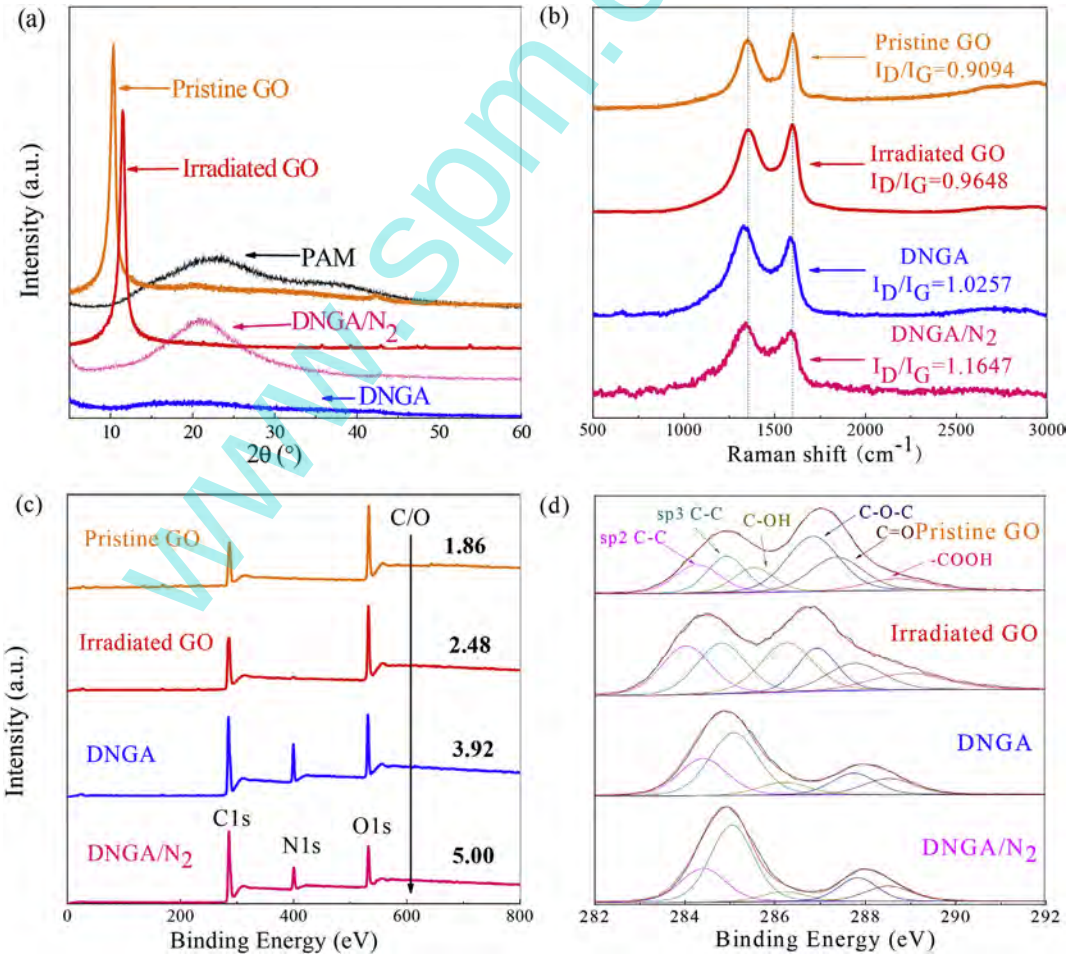

Fig. 5. XRD diffraction patterns of PAM, pristine GO, irradiated GO, DNGA and DNGA/N_2 (a); Raman spectra with I_D/I_G ratio (b), XPS full spectra (c) and C1s spectra (d) of pristine GO, irradiated GO, DNGA and DNGA/N_2.

Table 1
Analysis of the deconvoluted C1s peaks from XPS of the obtained products.

XPS C1s peaks	C1s relative atomic percentage, %						
	C–C sp2	C–C sp3	C–OH	C–N	C–O–C	C=O	–COOH
BE(eV)	284.0–284.4	284.5–285.1	286.2–286.7		286.8–287.3	287.5–288.2	288.5-289
Pristine GO	14.28	15.35	11.01	–	31.52	19.75	8.09
Irradiated GO	20.10	20.86	21.49	–	14.32	12.83	10.40
DNGA	24.78	42.06	8.58		–	13.25	11.33
DNGA/N2	21.19	49.30	–	6.08	–	16.22	7.21

intensity ratio of D to G peak was denoted as I_D/I_G, and the value indicated structural disorder caused by defects. Compared to pristine GO and irradiated GO, the position of G peak of DNGA was unchanged, while its D peak showed a notable red-shifting from 1358 to 1330 cm^{-1}. After irradiation in water, the I_D/I_G value of GO increased from 0.9094 to 0.9648. This result suggested that γ-ray irradiation decreased the average size of sp^2 carbon domains, which were induced by the formation of increasing smaller graphitic domains during the irradiation process [51,52]. The increased I_D/I_G value of DNGA indicated that more defects were brought into DNGA during the irradiation polymerization, and a largely disordered structure further implied that polyacrylamide-modified graphene sheets were successfully prepared. Owing to the formation of 3D graphene network in DNGA, new domains of conjugated carbon atoms were formed, and the distortions increased along with the removal of oxygen-containing groups [53]. The I_D/I_G values of DNGA and DNGA/N_2 were 1.0257 and 1.1647, respectively, which suggested that thermal-annealing led to the transformation of organic carbon chains, and promoted the reduction of DNGA [54]. The conductivity of DNGA increased from 0.212 to 8.49 S/m after thermal annealing, which further demonstrated the above viewpoint.

XPS spectra of the obtained products were shown in Fig. 5(c–d) to further analyze the evidence of reaction mechanism. After γ-ray irradiation, the content of nitrogen in DNGA was close to 15%. Furthermore, the C1s XPS spectra were fitted by a Gaussian–Lorentzian peak shape in Fig. 5(d) to provide rich information about the functional groups of GO and DNGA, and the results were recorded in Table 1. As shown in Fig. 5(d), for C1s core shell spectrum of irradiated GO, the intensity of C–OH absorption peak increased significantly, but it was opposite to that of C–O–C and C=O. The C/O atomic ratio of irradiated GO was obviously larger than that of pristine GO, which was consistent with previous research [46]. This phenomenon manifested that the γ-rays brought double-side effects to GO, which was in line with TGA [42]. The existence of AM increased the C/O atomic ratio, and facilitated the generation of –COOH and the reduction of C=O. As the weakest oxygen functional groups, C–O–C was reduced thoroughly. Besides, the introduction of AM caused many defects, and C–OH decreased sharply [55]. After thermal-annealing process, the amounts of sp^2 C–C reduced while that of sp^3 C–C increased significantly. The content of C–OH in DNGA/N_2 changed slightly because the binding energy of C–N was similar to that of C–OH. The results showed that thermal treatment induced the carbonation of organic crosslinking of PAM, and promoted the nitrogen doping of polyacrylamide-modified graphene sheets. The transformation of –COOH and diminishment of C–OH illustrated that oxygen functional groups can be selectively reduced by γ-ray irradiation and thermal treatment.

Unidirectional compression tests were conducted on DNGA and DNGA/N_2, and the compressive stress–strain curves were shown in Fig. 6. The compressive stress–strain curve of DNGA in Fig. 6(a) manifested three regimes of deformation: (i) nearly linear elastic regime at low stress, corresponding to bending of the cell walls; (ii) relatively flat stress plateau, corresponding to elastic buckling of cell walls; (iii) and abrupt stress increasing regime, corresponding to densification of cells [56]. According to the linear region in Fig. 6(a), the Young's modulus of DNGA was 1.70 MPa. DNGA possessed a compressive strength of ~1.45 MPa at 80% compression strain, which was far higher than that of other 3D graphene networks [38]. The compressive strength of DNGA was enlarged up to three-fold compared with that of graphene/polypyrrole aerogel which was prepared by self-assembled method in Ye's study [57]. Due to super performance of γ-rays, 3D graphene network could be built and induce the formation of PAM network simultaneously. The coordination of these two intertwined networks made the

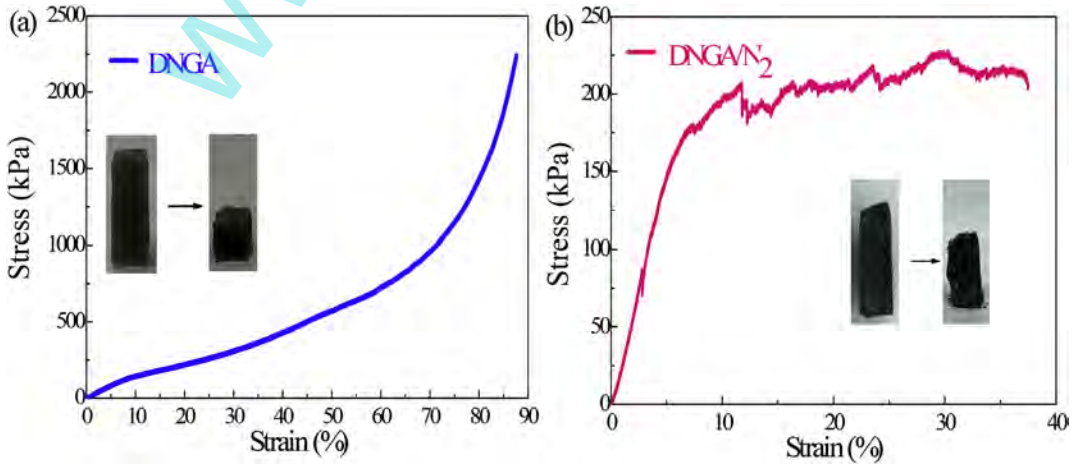

Fig. 6. Compressive stress–strain curves of DNGA (a) and DNGA/N_2 (b). The insets are their digital images before and after the compression tests.

Table 2
Compression performance of different 3D graphene network materials.

Sample	Compositions (besides GO)	Method	Scale	Fabrication process	Density/ $Kg \cdot m^{-3}$	Young's modulus/ kPa	Specific modulus/ $N \cdot m \cdot g^{-1}$	Compressive strength/ kPa	Specific strength/ $N \cdot m \cdot g^{-1}$	Conduc ivity/$S \cdot m^{-1}$	Ref.
DNGA	AM	γ-Ray irradiation	Large	Easy	38.57	1698	44.024	1451 (strain = 80%)	37.62	0.21	This
DNGA/N_2					15.71	2934	186.76	207.94(strain = 13%)	13.24	8.49	work
Graphene sponge	Detergent	Template	Medium	Medium	11.4	–	–	<0.06(strain = 30%)	0.01	–	[17]
Graphene aerogel	PPD	Reduction-assembly	Small	Complex	14.2	856	60.28	146.00	10.28	1.0	[27]
Graphene aerogel	CNT/hydrazine	Sol-cryo	Medium	Complex	5.6	<0.1	<0.1	~2	0.36	0.6	[59]
3D graphene	Reducing agent	Chemical reduction	Small	Medium	18	130	7.22	28	1.56	87	[60]
Graphene aerogel	L-ascorbic acid	Sol–gel	Small	Easy	47.6	1100	23.11	150	3.15	100	[61]
Graphene fiber	Hydroiodic acid			Complex	71	1100	15.49	3300(strain = 70%)	46.48	2000	[62]
Graphene monolith	Ascorbic acid	Self-assembly	Small	Complex	5.1	20.00	3.92	18.55(strain = 80%)	3.64	12	[56]
Graphene aerogel	Polypyrrole				84	–	–	~350 (strain = 70%)	4.17	–	[57]
Graphene network	PVA/sucrose				~1.5	–	–	~1	0.67	40	[63]
Grapheme aerogel	CNT/polypyrrole	Freeze-drying	Small	Complex	8	–	–	9(strain = 80%)	1.13	–	[64]
Graphene foam	–		Medium	Easy	5.5	–	–	16(strain = 60%)	2.91	3–10	[65]
Graphene aerogel	BDGE/TETA		Medium	Easy	92.90	–	–	231(strain = 75%)	2.49	–	[66]
Graphene hydrogel	–	Hydrothermal	Small	Medium	–	26–310	–	2.50–26.00	–	0.47–0.51	[21]
Graphene monolith	Hexane			Complex	12.32	42.29	3.43	31.94(strain = 50%)	2.59	1.76	[24]
Graphene aerogel	Ammonia			Medium	16	4.8	0.3	152.00	9.50	–	[67]
Graphene sponge	Thiourea			Medium	–	–	–	140.00(strain = 82%)	–	–	[68]
Graphene hydrogel	Phenolic acids			Easy	12.9–13.5	180–196	~15	110–150	8.53–11.11	33.3–33.9	[69]
Graphene hydrogel	oPDA			Easy	22.6	–	–	36.00	1.59	–	[70]

obtained DNGA possess higher density of crosslinking than some 3D graphene networks prepared by other methods. As shown in Fig. 6(b), before compressive strain reached 5%, the stress–strain curve of DNGA/N_2 was in linear relationship, and its Young's modulus and partial break stress were 2.93 MPa and 207.9 kPa, respectively. In the compressive stress–strain curve of DNGA/N_2, a slope was slowly rising until compressive strain reached 13%. Afterwards, the compressive stress value changed little due to the destruction of the architectures. As digital images shown in Fig. 6, the slippage of double network brought an irreversible compression rather than collapse. However, attributing to the disappearance of toughness PAM network, DNGA/N_2 was compressed accompanying with a visible large area of damage. The phenomena were consistent with the changed values of Young's modulus and compressive strength, which demonstrated that thermal treatment inhibited organic carbon chains sliding and promoted the formation of inorganic carbon chains. As the compressive property was typically associated to the density, the comparison of our samples with some other 3D graphene networks for Young's modulus and compressive strength relating to density was listed in Table 2. The values of Young's modulus of DNGA and DNGA/N_2 were one to twice higher than those of graphene gels [58]. The high Young's modulus and robust compressive strength of DNGA were attributed to the double network with highly efficiently crosslinking by γ-ray irradiation. Furthermore, the outstanding compressive property of DNGA and DNGA/N_2 broadened the application field of 3D graphene networks, especially for the reinforcement of nanocomposites.

To better understand the structure-property relationship of DNGA and DNGA/N_2, below we provided our opinions regarding the influence of the double network structure and thermal-annealing process on the compressive property of DNGA and DNGA/N_2. Owing to the efficacious construction of crosslinking polyacrylamide-modified graphene, the graphene network, as the first network, not only reinforced compressive strength of DNGA, but also supplied with framework to promote the formation of PAM network. The inference was testified by the previous analysis of the SEM images in Fig. 4(a–d), which indicated that DNGA had stable porous structure rather than the lamellar structure of pure PAM. Also, previous study [71] has shown that the formation of double network endowed high toughness and strength to the architectures because relatively long polymer chains in the second network allowed for more phorogenesis within and between the two networks. Furthermore, the interaction of hydrogen bonding and the interpenetration of DNGA slowed down macroscopic crack propagation throughout the entire network [72]. After thermal-annealing process, the density and compressive strength of DNGA/N_2 were remarkably decreased, which was attributed to the disappearance of organic carbon chains, the further reduction of modified graphene network, and the breakage of hydrogen bonding. However, the Young's modulus of DNGA/N_2 significantly increased, which implied that the generation of amorphous carbon remedied the defect position to enhance the stiffness of DNGA/N_2. The compressive property of architectures may be dependent on the ratio of graphene/amorphous carbon. According to TGA results, we have calculated the ratio of graphene/amorphous carbon in DNGA/N_2 which was 0.72. Hence the most dominant strengthening mechanism of DNGA was the synergistic effect between high-strength graphene network and high-toughness PAM network, and the adhesive characteristic of amorphous carbon reinforced graphene network, which improved Young's modulus of DNGA/N_2.

4. Conclusions

This work presented a straightforward method for one-step fabricating DNGA from GO and AM mixture solution by γ-ray irradiation at atmospheric pressure and ambient temperature. Based on the FTIR, TGA, SEM and other measurements, it can be concluded that GO was successfully exfoliated, and reduction and crosslinking of the modified graphene sheets occurred simultaneously, resulting in the formation of 3D graphene network. Meanwhile, interpenetration of the graphene network and PAM network constituted the double network structure. Owing to the high density of covalent bonds and organic carbon chains in DNGA, the as-synthesized DNGA possessed a stable macroporous structure at high temperature (≥800 °C) and superior mechanical properties (Young's modulus 1.70 MPa and compressive strength 1.45 MPa). Compared with those reported in recent literatures, the Young's modulus and compressive strength of DNGA were increased about two times and quadruple, respectively. After thermal-annealing process, the conductivity of DNGA/N_2 was increased to 8.49 S/m, which was almost fortyfold to that of DNGA (0.212 S/m).Young's modulus of DNGA/N_2 was increased to 2.93 MPa, while the compressive strength was decreased to 207.9 kPa. These results demonstrated that thermal treatment promoted further reduction of DNGA, and endowed DNGA/N_2 with the feature of high modulus by carbonization of organic carbon chains. As 3D graphene materials are currently being explored for a broad range of applications, γ-ray irradiation technique undoubtedly provides a large-scale engineered method for graphene self-enhancement materials with high mechanical strength, and offers opportunity to create new ultralight graphene-based nanocomposites. However, more work should be done to optimize the microstructure of DNGA, and verify the crosslinking sites between graphene and AM thoroughly due to the complex process of γ-ray irradiation.

Acknowledgment

The work was funded by the National Natural Science Foundation of China (11175130, 11575126 and 51502202).

References

[1] A.K. Geim, K.S. Novoselov, The rise of graphene, Nat. Mater. 6 (3) (2007) 183–191.
[2] Q. Li, P. Xu, W. Gao, S. Ma, G. Zhang, R. Cao, et al., Graphene/graphene-tube nanocomposites templated from cage-containing metal-organic frameworks for oxygen reduction in Li-O_2 batteries, Adv. Mater. 26 (9) (2014) 1378–1386.
[3] Y. Wang, Y. Li, L. Tang, J. Lu, J. Li, Application of graphene-modified electrode for selective detection of dopamine, Electrochem. Commun. 11 (4) (2009) 889–892.
[4] J. Yang, J. Wang, Y. Tang, D. Wang, X. Li, Y. Hu, et al., $LiFePO_4$-graphene as a superior cathode material for rechargeable lithium batteries: impact of stacked graphene and unfolded graphene, Energ. Environ. Sci. 6 (5) (2013) 1521–1528.
[5] W. Yuan, J. Chen, G. Shi, Nanoporous graphene materials, Mater. Today 17 (2) (2014) 77–85.
[6] Z. Jiang, J. Wang, L. Meng, Y. Huang, L. Liu, A highly efficient chemical sensor material for ethanol: Al_2O_3/graphene nanocomposites fabricated from graphene oxide, Chem. Commun. 47 (22) (2011) 6350–6352.
[7] W. Gao, G. Wu, M.T. Janicke, D.A. Cullen, R. Mukundan, J.K. Baldwin, et al., Ozonated graphene oxide film as a proton-exchange membrane, Angew. Chem. Int. Ed. 53 (14) (2014) 3588–3593.
[8] H. Bai, K. Sheng, P. Zhang, C. Li, G. Shi, Graphene oxide/conducting polymer composite hydrogels, J. Mater. Chem. 21 (46) (2011) 18653.
[9] D.R. Dreyer, S. Park, C.W. Bielawski, R.S. Ruoff, The chemistry of graphene oxide, Chem. Soc. Rev. 39 (1) (2010) 228–240.
[10] J. Yang, J. Wang, D. Wang, X. Li, D. Geng, G. Liang, et al., 3D porous $LiFePO_4$/graphene hybrid cathodes with enhanced performance for Li-ion batteries, J. Power Sources 208 (2012) 340–344.
[11] J. Wang, B. Li, T. Ni, T. Dai, Y. Lu, One-step synthesis of iodine doped polyaniline-reduced graphene oxide composite hydrogel with high capacitive properties, Compos. Sci. Technol. 109 (2015) 12–17.
[12] X. Ji, L. Cui, Y. Xu, J. Liu, Non-covalent interactions for synthesis of new graphene based composites, Compos. Sci. Technol. 106 (2015) 25–31.
[13] L. Zhang, G. Shi, Preparation of highly conductive graphene hydrogels for fabricating supercapacitors with high rate capability, J. Phys. Chem. C 115 (34) (2011) 17206–17212.

[14] Z. Chen, W. Ren, L. Gao, B. Liu, S. Pei, H.-M. Cheng, Three-dimensional flexible and conductive interconnected graphene networks grown by chemical vapour deposition, Nat. Mater. 10 (6) (2011) 424–428.
[15] D. Wang, X. Li, J. Yang, J. Wang, D. Geng, R. Li, et al., Hierarchical nano-structured core-shell Sn@C nanoparticles embedded in graphene nanosheets: spectroscopic view and their application in lithium ion batteries, Phys. Chem. Chem. Phys. 15 (10) (2013) 3535–3542.
[16] Y.-E. Shin, Y.J. Sa, S. Park, J. Lee, K.-H. Shin, S.H. Joo, et al., An ice-templated, pH-tunable self-assembly route to hierarchically porous graphene nano-scroll networks, Nanoscale 6 (16) (2014) 9734–9741.
[17] R. Zhang, Y. Cao, P. Li, X. Zang, P. Sun, K. Wang, et al., Three-dimensional porous graphene sponges assembled with the combination of surfactant and freeze-drying, Nano Res. 7 (10) (2014) 1477–1487.
[18] W. Lv, C. Zhang, Z. Li, Q.-H. Yang, Self-assembled 3D graphene monolith from solution, J. Phys. Chem. Lett. 6 (4) (2015) 658–668.
[19] V. Chabot, D. Higgins, A. Yu, X. Xiao, Z. Chen, J. Zhang, A review of graphene and graphene oxide sponge: material synthesis and applications to energy and the environment, Energy Environ. Sci. 7 (5) (2014) 1564–1596.
[20] C. Li, G. Shi, Three-dimensional graphene architectures, Nanoscale 4 (18) (2012) 5549–5563.
[21] Y. Xu, K. Sheng, C. Li, G. Shi, Self-assembled graphene hydrogel via a one-step hydrothermal process, ACS nano 4 (7) (2010) 4324–4330.
[22] Y. Zhang, Y. Huang, T. Zhang, H. Chang, P. Xiao, H. Chen, et al., Broadband and tunable high-performance microwave absorption of an ultralight and highly compressible graphene foam, Adv. Mater. 27 (12) (2015) 2049–2053.
[23] H.N. Tien, N.T.M. Hien, E.-S. Oh, J. Chung, E.J. Kim, W.M. Choi, et al., Synthesis of a highly conductive and large surface area graphene oxide hydrogel and its use in a supercapacitor, J. Mater. Chem. A 1 (2) (2013) 208–211.
[24] Y. Li, J. Chen, L. Huang, C. Li, J.D. Hong, G. Shi, Highly compressible macro-porous graphene monoliths via an improved hydrothermal process, Adv. Mater. 26 (28) (2014) 4789–4793.
[25] C. Li, G. Shi, Functional gels based on chemically modified graphenes, Adv. Mater. 26 (24) (2014) 3992–4012.
[26] S. Nardecchia, D. Carriazo, M.L. Ferrer, M.C. Gutiérrez, F. del Monte, Three dimensional macroporous architectures and aerogels built of carbon nano-tubes and/or graphene: synthesis and applications, Chem. Soc. Rev. 42 (2) (2013) 794–830.
[27] G. Tang, Z.-G. Jiang, X. Li, H.-B. Zhang, A. Dasari, Z.-Z. Yu, Three dimensional graphene aerogels and their electrically conductive composites, Carbon 77 (2014) 592–599.
[28] L. Chen, Z. Xu, J. Li, Y. Li, M. Shan, C. Wang, et al., A facile strategy to prepare functionalized graphene via intercalation, grafting and self-exfoliation of graphite oxide, J. Mater. Chem. 22 (27) (2012) 13460–13463.
[29] L. Chen, Z. Xu, J. Li, B. Zhou, M. Shan, Y. Li, et al., Modifying graphite oxide nanostructures in various media by high-energy irradiation, Rsc Adv. 4 (2) (2014) 1025–1031.
[30] C.H. Zhu, Y. Lu, J. Peng, J.F. Chen, S.H. Yu, Photothermally sensitive poly (N-isopropylacrylamide)/graphene oxide nanocomposite hydrogels as remote light-controlled liquid microvalves, Adv. Funct. Mater. 22 (19) (2012) 4017–4022.
[31] H.P. Cong, P. Wang, S.H. Yu, Highly elastic and superstretchable graphene oxide/polyacrylamide hydrogels, Small 10 (3) (2014) 448–453.
[32] Y. Zhang, H.-L. Ma, Q. Zhang, J. Peng, J. Li, M. Zhai, et al., Facile synthesis of well-dispersed graphene by γ-ray induced reduction of graphene oxide, J. Mater. Chem. 22 (26) (2012) 13064–13069.
[33] Z. Xu, Y. Zhang, X. Qian, J. Shi, L. Chen, B. Li, et al., One step synthesis of polyacrylamide functionalized graphene and its application in Pb(II) removal, Appl. Surf. Sci. 316 (2014) 308–314.
[34] J.P. Gong, Y. Katsuyama, T. Kurokawa, Y. Osada, Double-network hydrogels with extremely high mechanical strength, Adv. Mater. 15 (14) (2003) 1155–1158.
[35] Q. Chen, H. Chen, L. Zhu, J. Zheng, Fundamentals of double network hydrogels, J. Mater. Chem. B 3 (18) (2015) 3654–3676.
[36] C. Shi, L. Chen, Z. Xu, Y. Jiao, Y. Li, C. Wang, et al., Monitoring influence of chemical preparation procedure on the structure of graphene nanosheets, Phys. E 44 (7) (2012) 1420–1424.
[37] D. Wang, X. Li, J. Wang, J. Yang, D. Geng, R. Li, et al., Defect-rich crystalline SnO_2 immobilized on graphene nanosheets with enhanced cycle performance for Li ion batteries, J. Phys. Chem. C 116 (42) (2012) 22149–22156.
[38] N. Zhang, R. Li, L. Zhang, H. Chen, W. Wang, Y. Liu, et al., Actuator materials based on graphene oxide/polyacrylamide composite hydrogels prepared by in situ polymerization, Soft Matter 7 (16) (2011) 7231–7239.
[39] D. Choi, O.-M. Lee, S. Yu, S.-W. Jeong, Gamma radiolysis of alachlor aqueous solutions in the presence of hydrogen peroxide, J. Hazard. Mater. 184 (1) (2010) 308–312.
[40] V.H. Pham, H.D. Pham, T.T. Dang, S.H. Hur, E.J. Kim, B.S. Kong, et al., Chemical reduction of an aqueous suspension of graphene oxide by nascent hydrogen, J. Mater. Chem. 22 (21) (2012) 10530–10536.
[41] C.K. Chua, M. Pumera, Chemical reduction of graphene oxide: a synthetic chemistry viewpoint, Chem. Soc. Rev. 43 (1) (2014) 291–312.
[42] W. Chen, Z. Zhu, S. Li, C. Chen, L. Yan, Efficient preparation of highly hydro-genated graphene and its application as a high-performance anode material for lithium ion batteries, Nanoscale 4 (6) (2012) 2124–2129.
[43] S. Park, J. An, R.D. Piner, I. Jung, D. Yang, A. Velamakanni, et al., Aqueous suspension and characterization of chemically modified graphene sheets, Chem. Mater. 20 (21) (2008) 6592–6594.
[44] S. Sun, P. Wu, A one-step strategy for thermal-and pH-responsive graphene oxide interpenetrating polymer hydrogel networks, J. Mater. Chem. 21 (12) (2011) 4095–4097.
[45] C. Wang, Q. Jin, Y. Wang, H. Yin, H. Xie, R. Cheng, A green route to prepare graphite oxide-poly(acrylic acid) and poly(acrylamide) hybrids under γ-ray irradiation, Mater. Lett. 68 (2012) 280–282.
[46] H. Jin, L. Chen, K. Zheng, Z. Xu, J. Shi, B. Zhou, et al., Super-high interlayer spacing of graphite oxide obtained by γ-ray irradiation in air, J. Mater. Sci. 49 (2) (2014) 827–832.
[47] M.A. Haque, T. Kurokawa, J.P. Gong, Super tough double network hydrogels and their application as biomaterials, Polymer 53 (9) (2012) 1805–1822.
[48] H. Hu, Z. Zhao, W. Wan, Y. Gogotsi, J. Qiu, Ultralight and highly compressible graphene aerogels, Adv. Mater. 25 (15) (2013) 2219–2223.
[49] J. Shen, B. Yan, T. Li, Y. Long, N. Li, M. Ye, Study on graphene-oxide-based polyacrylamide composite hydrogels, Compos. Part A Appl. Sci. 43 (9) (2012) 1476–1481.
[50] M. Pimenta, G. Dresselhaus, M.S. Dresselhaus, L. Cancado, A. Jorio, R. Saito, Studying disorder in graphite-based systems by Raman spectroscopy, Phys. Chem. Chem. Phys. 9 (11) (2007) 1276–1290.
[51] M.S. Dresselhaus, A. Jorio, M. Hofmann, G. Dresselhaus, R. Saito, Perspectives on carbon nanotubes and graphene Raman spectroscopy, Nano Lett. 10 (3) (2010) 751–758.
[52] S. Dannefaer, A. Pu, V. Avalos, D. Kerr, Annealing of monovacancies in electron and γ-irradiated diamonds, Phys. B Condens. Matter 308 (2001) 569–572.
[53] X. Song, L. Lin, M. Rong, Y. Wang, Z. Xie, X. Chen, Mussel-inspired, ultralight, multifunctional 3D nitrogen-doped graphene aerogel, Carbon 80 (2014) 174–182.
[54] T. Van Khai, H.G. Na, D.S. Kwak, Y.J. Kwon, H. Ham, K.B. Shim, et al., Significant enhancement of blue emission and electrical conductivity of N-doped gra-phene, J. Mater. Chem. 22 (34) (2012) 17992–18003.
[55] D. Yang, A. Velamakanni, G. Bozoklu, S. Park, M. Stoller, R.D. Piner, et al., Chemical analysis of graphene oxide films after heat and chemical treatments by X-ray photoelectron and Micro-Raman spectroscopy, Carbon 47 (1) (2009) 145–152.
[56] L. Qiu, J.Z. Liu, S.L. Chang, Y. Wu, D. Li, Biomimetic superelastic graphene-based cellular monoliths, Nat. Commun. 3 (2012) 1241.
[57] S. Ye, J. Feng, Self-Assembled Three-dimensional hierarchical graphene/pol-ypyrrole nanotube hybrid aerogel and its application for supercapacitors, ACS Appl. Mater. Inter. 6 (12) (2014) 9671–9679.
[58] W. Yao, C. Geng, D. Han, F. Chen, Q. Fu, Strong and conductive double-network graphene/PVA gel, Rsc Adv. 4 (2014) 39588–39595.
[59] H. Sun, Z. Xu, C. Gao, Multifunctional, ultra-flyweight, synergistically assem-bled carbon aerogels, Adv. Mater. 25 (18) (2013) 2554–2560.
[60] W. Chen, L. Yan, In situ self-assembly of mild chemical reduction graphene for three-dimensional architectures, Nanoscale 3 (8) (2011) 3132–3137.
[61] X. Zhang, Z. Sui, B. Xu, S. Yue, Y. Luo, W. Zhan, et al., Mechanically strong and highly conductive graphene aerogel and its use as electrodes for electro-chemical power sources, J. Mater. Chem. 21 (18) (2011) 6494–6497.
[62] Z. Xu, Y. Zhang, P. Li, C. Gao, Strong, conductive, lightweight, neat graphene aerogel fibers with aligned pores, ACS Nano 6 (8) (2012) 7103–7113.
[63] S. Barg, F.M. Perez, N. Ni, P. do Vale Pereira, R.C. Maher, E. Garcia-Tuñon, et al., Mesoscale assembly of chemically modified graphene into complex cellular networks, Nat. Commun. 5 (2014) 4328.
[64] C. Wang, X. He, Y. Shang, Q. Peng, Y. Qin, E. Shi, et al., Multifunctional gra-phene sheet–nanoribbon hybrid aerogels, J. Mater. Chem. A 2 (36) (2014) 14994–15000.
[65] J. Kuang, L. Liu, Y. Gao, D. Zhou, Z. Chen, B. Han, et al., A hierarchically structured graphene foam and its potential as a large-scale strain-gauge sensor, Nanoscale 5 (24) (2013) 12171–12177.
[66] S. Ye, J. Feng, P. Wu, Highly elastic graphene oxide–epoxy composite aerogels via simple freeze-drying and subsequent routine curing, J. Mater. Chem. A 1 (10) (2013) 3495–3502.
[67] Z. Han, Z. Tang, P. Li, G. Yang, Q. Zheng, J. Yang, Ammonia solution strengthened three-dimensional macro-porous graphene aerogel, Nanoscale 5 (12) (2013) 5462–5467.
[68] J. Zhao, W. Ren, H.-M. Cheng, Graphene sponge for efficient and repeatable adsorption and desorption of water contaminations, J. Mater. Chem. 22 (38) (2012) 20197–20202.
[69] J.S. Chung, E.J. Kim, S.H. Hur, The molecular level control of three-dimensional graphene oxide hydrogel structure by using various diamines, Chem. Eng. J. 246 (2014) 64–70.
[70] J. Wang, Z. Shi, J. Fan, Y. Ge, J. Yin, G. Hu, Self-assembly of graphene into three-dimensional structures promoted by natural phenolic acids, J. Mater. Chem. 22 (42) (2012) 22459–22466.
[71] T. Nakajima, Y. Fukuda, T. Kurokawa, T. Sakai, U.-I. Chung, J.P. Gong, Synthesis and fracture process analysis of double network hydrogels with a well-defined first network, ACS Macro Lett. 2 (6) (2013) 518–521.
[72] H. Tsukeshiba, M. Huang, Y.-H. Na, T. Kurokawa, R. Kuwabara, Y. Tanaka, et al., Effect of polymer entanglement on the toughening of double network hydrogels, J. Phys. Chem. B 109 (34) (2005) 16304–16309.